

THESIS WORK

Modeling the Cross Effect Between Circadian Rhythms and Cell Cycle on Cell Differentiation in Intestinal Crypts

FÜLEKI, Máté

Molecular Bionics Engineering BSc

Supervisors: Dr. CSIKÁSZ-NAGY, Attila

Dr. JUHÁSZ, János

2024

THESIS PROPOSAL FORM

Name (Neptun ID): **Füleki Máté (BE2T5W)**

Study program (ID): **Molecular Bionics Engineering BSc (IANI-MB)**

Supervisor

Dr. Csikász-Nagy Attila István (inner supervisor)

Dr. Juhász János (inner supervisor)

Thesis

Title:

Modeling the Cross Effect Between Circadian Rhythms and Cell Cycle on Cell Differentiation in Intestinal Crypts

Summary of the thesis:

The aim of the project is to create a computational model of an intestinal crypt detailed enough to unveil cross-effect methodologies between the circadian clock and the cell cycle. Multiple signaling pathways will be added to this intestinal crypt tissue model, related to circadian regulation and intercellular communication. After the model is finished a series of cell proliferation simulations will be conducted, followed by the analysis of the results.

Tasks:

- Reviewal of relevant literature on cell cycle, circadian clock and their cross effects
- Development of specific programming and modeling skills for the model
- Modeling of proliferation irregularity effect of faulty circadian system
- Programming of intercellular signal transduction
- Modeling the adaptation of circadian signaling pathways based on external signals
- Comparison of simulation results to real-life research data
- Drawing result-based conclusions on the cross effects of the cell cycle and circadian rhythms

Date of application: **11.09.2024**

Date of acceptance: **24.09.2024**

Date: Budapest, 10.12.2024

Declaration of Authenticity

I, undersigned Máté Fülekí, student of the Faculty of Information Technology and Bionics at the Pázmány Péter Catholic University, hereby certify that this thesis was written without any unauthorized help, solely by me and I used only the referenced sources. Every part, which is quoted exactly or in a paraphrased manner, is indicated clearly with a reference. I have not submitted this thesis anywhere else.



Signature of student

Abstract

The cell cycle and circadian rhythm are determined by the temporal changes and activities of various signaling factors. Significant roles in cell proliferation and differentiation are played by the WNT signaling system, the Cyclin-Dependent Kinase (CDK) signaling system, and the Mitogen-Activated Protein Kinase (MAPK) system. In the regulation of the circadian rhythm, the CLOCK-BMAL1 signaling system and Casein Kinase 1 (CK1) are involved. Although these complex biological processes are built on distinct time-dependent signaling systems, there is crosstalk between their pathways, leading to interdependence.

In the case of intestinal villi, the processes of cell proliferation and differentiation can be studied based on their structure. In colorectal cancer, DNA damage influences the signaling pathways that regulate cell proliferation. We hypothesize that the interaction between the circadian rhythm and the cell cycle can enhance the effectiveness of drug treatments targeting cell division.

This thesis investigates the interplay between these biological systems through a computational model designed to simulate cell proliferation, differentiation, and movement in the mammalian intestinal crypt. The model integrates mathematical representations of circadian signaling pathways, cell cycle regulation, and intercellular communication, with a focus on the WNT and BMP gradients.

Contents

Abstract	6
1 Introduction	9
1.1 Motivation and medical application	9
1.2 Cell cycle	10
1.3 Circadian clock	11
1.4 Cell types of the intestinal crypt tissue	13
2 Methods	17
2.1 Evaluation of decision options	17
2.2 Grids	17
2.3 Working principle	19
2.3.1 Cell age counter	19
2.3.2 Intracellular functions	21
2.3.3 Exocytosis – Diffusion - Endocytosis	24
2.3.4 Cell fate analysis	26
2.3.5 Death function	28
2.3.6 Division function	28
2.4 Visualization	30
3 Results	31
3.1 Simulation 1	31
3.1.1 Evaluation of Simulation 1	33
3.2 Simulation 2	34
3.2.1 Evaluation of Simulation 2	34
3.3 Simulation 3	36
3.3.1 Evaluation of Simulation 3	36
3.4 Simulation 4	36
3.4.1 Evaluation of Simulation 4	37

4 Summary	40
4.1 Results	40
4.2 Future plans	40
4.2.1 Room for improvement	40
4.2.2 Project future	41
Bibliography	45
A	46

Chapter 1

Introduction

1.1. Motivation and medical application

Disruptions in circadian rhythms, caused by factors such as shift work or jet lag, are associated with significant alterations in crypt-villus homeostasis. Studies have shown that circadian misalignment can lead to hyperproliferation of intestinal stem cells (ISCs), impaired differentiation, creating a predisposition to colorectal cancer [1]. Furthermore, clock-regulated signaling pathways like Wnt and Notch become deregulated, exacerbating tumorigenesis and inflammatory conditions [2].

Dysregulation of the cell cycle is the basis of cancer. Mutations in genes coding key regulators, such as p53, cyclin D1, and CDK inhibitors like p16, result in uncontrolled proliferation and genomic instability. Therapeutic strategies targeting the cell cycle have emerged as promising cancer treatments. For example, CDK4/6 inhibitors like palbociclib are used in breast cancer to arrest tumor cells in G1. Additionally, targeting checkpoint kinases or the DDR with drugs such as PARP inhibitors exploits the vulnerabilities of cancer cells with defective repair mechanisms.[3][4]

Advances in understanding the molecular basis of the cell cycle continue to reveal novel therapeutic opportunities. By elucidating the interplay between cell cycle regulation and cellular signaling, researchers aim to develop precise, effective treatments for proliferative diseases.

Recent advances in chronotherapy (strategic timing of drug delivery) suggest that targeting the circadian clock could improve treatment outcomes for intestinal disorders. For example, delivering chemotherapeutic agents or probiotics at circadian-optimal times can enhance efficacy and reduce toxicity by aligning treatment with the natural rhythms of the crypt-villus axis.[5]

Learning more about the coupling of cell cycle and circadian rhythms is crucial from both a scientific and a medical standpoint. The focus of this project is to contribute to general knowledge about the behaviour of intestinal tissues in a variety of molecular states.

1.2. Cell cycle

The cell cycle is a complex, tightly regulated process that governs the growth and division of cells, ensuring the accurate replication and distribution of genetic material. It plays a central role in tissue maintenance, development, and repair. This section is a quick overview of the general cell cycle, and its molecular processes, introducing molecules implemented in my work.

The cell cycle consists of four main phases: G1 (Gap 1), S (Synthesis), G2 (Gap 2), and M (Mitosis). An additional phase, G0, represents a quiescent state in which cells exit the cycle and stop dividing. This progression is orchestrated by cyclin-dependent kinases (CDKs) and their regulatory subunits, cyclins, which function as the master regulators of cell cycle transitions.

The G1 Phase is a preparatory stage where the cell grows and accumulates the resources necessary for DNA replication. During this phase, external signals such as growth factors play a crucial role in determining whether the cell progresses through the cycle or enters G0. At the molecular level, the retinoblastoma protein (pRB) is a key gatekeeper. In its hypophosphorylated state, pRB binds and inhibits the transcription factor E2F, preventing the expression of genes required for DNA synthesis. Phosphorylation of pRB by cyclin D-CDK4/6 complexes releases E2F, enabling the cell to commit to DNA replication.

The S Phase marks the synthesis of DNA, where the genome is duplicated with high fidelity. This process is initiated at replication origins, which are activated in a regulated manner to ensure each segment of DNA is replicated once and only once. Cyclin A-CDK2 complexes drive this phase by phosphorylating key replication factors, including helicases and DNA polymerases. Proliferating cell nuclear antigen (PCNA) acts as a sliding clamp, stabilizing DNA polymerase and ensuring processivity during replication. Checkpoints monitor for DNA damage or replication errors, and mechanisms such as mismatch repair correct any mistakes.

The G2 Phase provides a window for the cell to grow further and prepare for mito-

sis. During this phase, cyclin B-CDK1 complexes, also known as maturation-promoting factors (MPFs), accumulate and are activated. This activation is tightly regulated; inhibitory phosphorylation of CDK1 by Wee1 kinase is removed by Cdc25 phosphatases, allowing the cell to proceed to mitosis. The G2/M checkpoint ensures that DNA damage or incomplete replication is resolved before mitotic entry, with checkpoint kinases such as CHK1 and CHK2 playing a critical role.

The M Phase, or mitosis, is the culmination of the cell cycle, where replicated chromosomes are segregated into two daughter cells. This phase is divided into several stages: prophase, prometaphase, metaphase, anaphase, and telophase. Key molecular players include the anaphase-promoting complex/cyclosome (APC/C), a ubiquitin ligase that triggers the degradation of securin, allowing separase to cleave cohesin complexes and separate sister chromatids.[6] Aurora kinases and spindle assembly checkpoint proteins, such as BubR1 and Cdc20, ensure that all chromosomes are correctly attached to the spindle before anaphase proceeds. Cytokinesis, the division of the cytoplasm, concludes the cell cycle. [7] [8]

1.3. Circadian clock

The circadian clock is a sophisticated biological mechanism that synchronizes physiological and behavioral processes with the 24-hour light-dark cycle. This evolutionary adaptation enables organisms to predict and respond to periodic environmental changes, influencing critical biological systems, including metabolism, immunity, and cellular homeostasis [9]. At its core, the circadian clock is driven by an intricate network of transcriptional-translational feedback loops (TTFLs) that regulate gene expression in a rhythmic manner.

Overview of molecular mechanisms

At the molecular level, circadian rhythms are orchestrated by core clock genes such as CLOCK, BMAL1, PER (Period), and CRY (Cryptochrome). The CLOCK and BMAL1 proteins form a heterodimeric complex that activates the transcription of PER and CRY genes. The PER and CRY proteins accumulate in the cytoplasm, dimerize, and translocate back into the nucleus, where they inhibit CLOCK-BMAL1 activity, creating a self-sustained oscillation (24 hours) [10]. Additional regulatory loops, such as the involvement of REV-ERB and ROR nuclear receptors, fine-tune these oscillations, linking the clock to metabolic and immune processes [10].

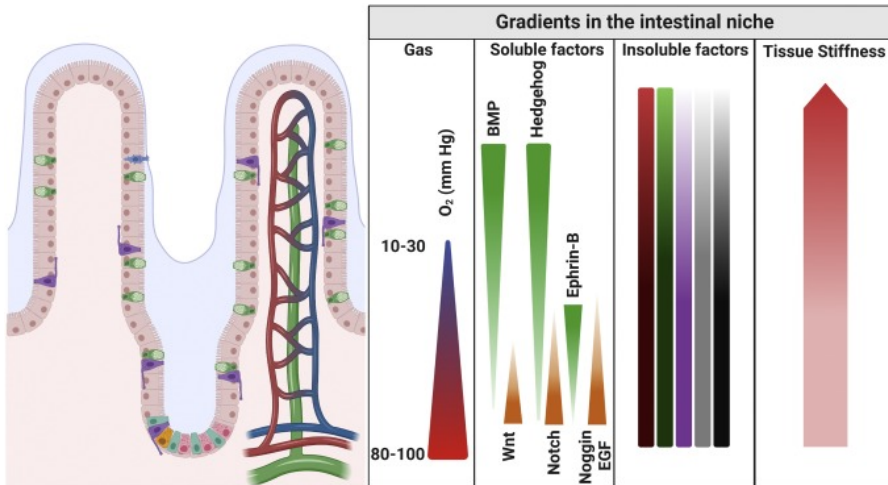


Figure 1.1: The diagram illustrates the gradients present in the intestinal crypt-villus axis. Wnt activity peaks at the crypt base, supporting intestinal stem cell maintenance and proliferation, while its gradient diminishes toward the villus. In contrast, BMP signaling intensifies toward the villus, promoting cell differentiation and inhibiting proliferation. This dynamic interplay between Wnt and BMP gradients establishes a balance between stem cell renewal and differentiation along the intestinal epithelium. Figure source:[12].

Circadian control in the intestinal crypt

The intestinal epithelium, one of the most rapidly renewing tissues in the body, is an excellent model for studying the intersection of circadian rhythms and cellular processes. The crypt-villus unit in the small intestine represents a spatial gradient of cellular differentiation, proliferation, and functional specialization. At the base of the crypt, ISCs reside in a niche regulated by gradients of signaling molecules such as Wnt, Notch, and BMP (bone morphogenetic protein). These stem cells give rise to progenitor cells that migrate upwards, differentiating into specialized cells (e.g., enterocytes, goblet cells, and Paneth cells) along the crypt-villus axis [11].

Circadian clocks play a vital role in modulating the crypt-villus gradient. Emerging evidence suggests that the rhythmic expression of clock genes impacts key signaling pathways that govern stem cell behavior and lineage specification. For instance, BMAL1 has been shown to regulate the Wnt/ β -catenin pathway, a critical driver of ISC proliferation and differentiation [2].

As cells migrate from the crypt base toward the villus tip, they transition from a proliferative state to a fully differentiated state. Circadian rhythms coordinate this process by regulating cell cycle phases, DNA repair mechanisms, and apoptosis in a time-dependent

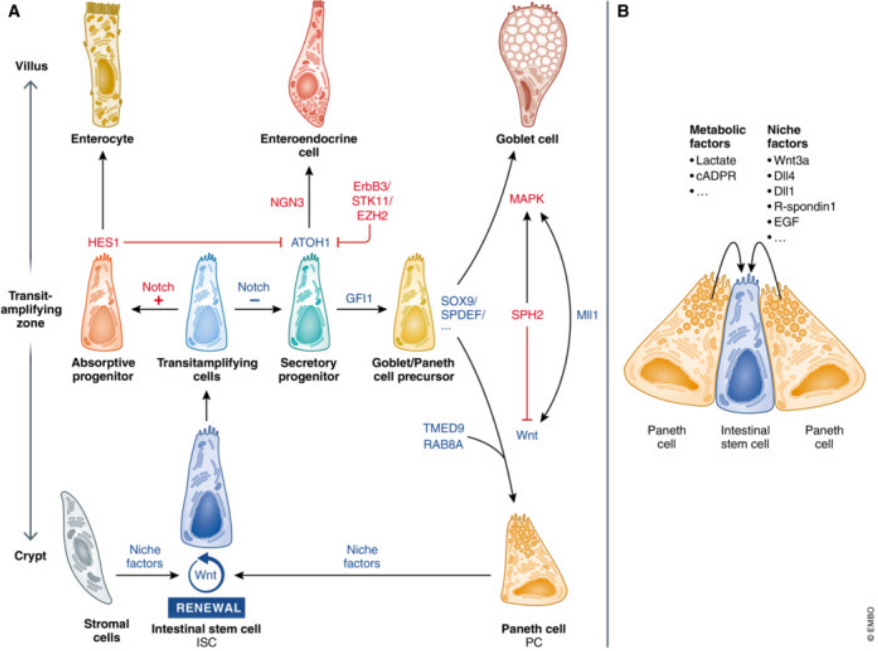


Figure 1.2: Cell differentiation along the crypt-villus axis. Cell types in the epithelium have different sensitivities to regulating signals. Notch and WNT signals maintain the ISC niche. Proliferation in the crypt constantly pushes cells upwards to- and from the the transit amplifying zone, prompting them to differentiate. The movement preserves the self renewal of the epithelium, while external signals keep the individual cell types from overpopulating. Figure source: [14]

manner [13]. Importantly, circadian disruption can impair this gradient, leading to imbalances in cell proliferation and differentiation.

1.4. Cell types of the intestinal crypt tissue

In this section I summarize the cellular diversity along the crypt-villus axis. Each of the following cell types are indispensable in modeling of the intestinal epithelium.

Intestinal stem cells Located at the base of the crypt, ISCs provide maintenance of the intestinal epithelium. They exhibit a constant ability to self-renew and are able to differentiate into other cell types, ensuring epithelial turnover. ISCs mostly divide asymmetrically, ensuring that one daughter cell retains stem cell properties while the other progresses to a transiently amplifying state. This balance is critical for maintaining a constant stem cell pool while providing a continuous source of new cells for the epithelium. ISCs express markers like Lgr5 and are sustained by the crypt niche, where signals

such as Wnt, Notch, and BMP modulate their activity.[15]

Transit amplifying cells (TA) (TA) cells represent the next stage in the differentiation hierarchy. These cells are positioned just above the stem cell zone and undergo rapid proliferation to produce a large number of progeny. Although transiently amplifying, these cells divide frequently before terminally differentiating into specialized cell types.[16][17]

Absorptive progenitors Differentiation of TA cells gives birth to absorptive and secretory lineages. Absorptive progenitors are intermediate cells in the differentiation pathway leading to enterocytes, the primary absorptive cells of the intestinal epithelium. These progenitors commit to the absorptive lineage under the influence of transcriptional cues such as HNF4 α , ultimately giving rise to cells that specialize in nutrient uptake and digestion.

Enterocytes Enterocytes specialize in nutrient absorption, utilizing their extensive brush border, a structure formed by densely packed microvilli. These microvilli are rich in enzymes such as sucrase-isomaltase and lactase, which facilitate the breakdown of complex carbohydrates into absorbable monosaccharides. Additionally, enterocytes transport amino acids, lipids, and vitamins across the epithelium, ensuring efficient uptake of nutrients into the bloodstream. This absorptive function is vital for sustaining the metabolic demands of the organism. Enterocytes also produce diffusive BMP signal molecules.[16][18]

Secretory progenitors Secretory progenitors are precursors to the secretory lineages, including goblet cells and Paneth cells. These progenitors are directed by transcription factors like Atoh1 (also known as Math1), which drive them towards producing cells involved in mucus secretion, antimicrobial defense, and hormone production. This specialization supports epithelial protection, immune responses, and regulatory functions within the gut.[15][19]

Goblet cells Goblet cells are integral to the protective mechanisms of the intestinal lining. They secrete mucins, which form a gel-like mucus layer that shields the epithelium from mechanical stress, microbial invasion, and chemical irritants. This mucus layer also facilitates the smooth passage of luminal contents, reducing the risk of epithelial damage.[18]

Type	Position	Number	Lifespan	End of Life	Division Time
S (Stem cell)	Crypt base	12-16	Inf.	Diff. to T	24h
T (Transit amplifying cell)	Crypt side	200-300	Inf.	Diff. to Ap or Sp	12h
Ap (Absorptive progenitor)	Upper crypt side	200-300	Inf.	Diff. to E	12h
Sp (Secretory progenitor)	Upper crypt side	200-300	Inf.	Diff. to G	48h
E (Enterocyte)	Villus	450-500	3-5 days	Shredding from villus top, Die	Ø
G (Goblet cell)	Villus	50-100	3-5 days	Shredding from villus top, Die	Ø
P (Paneth cell)	Crypt base	12-16	16(-28) days	Die	Ø

Table 1.1: Cell types with their positions, numbers, lifespans, end of life states, and division times. The data listed in Table 1.1 and Table 1.2 was discussed during project meetings, sourced from [14],[22],[23],[24] and was summarized by Dr. János Juhász.

Paneth cells Paneth cells can be found in various positions along the intestinal crypt. Post maturation process (migration) at the base of the crypt, Paneth cells perform two roles: defense and stem cell niche maintenance. They secrete antimicrobial peptides such as α -defensins, lysozyme, and RegIII γ , which help controlling the composition of the intestinal microbiota by targeting pathogenic organisms.[20] Additionally, Paneth cells provide essential niche signals, including Wnt and epidermal growth factor (EGF), which are crucial for the survival and proliferation of ISCs. This symbiotic relationship highlights the critical role of Paneth cells in both epithelial integrity and innate immunity. [21]

The number of transit amplifying, absorptive progenitor and secretory progenitor cells are relatively close, however data suggests a $n_T > n_{ap} > n_{sp}$ relation.[11]

Type	Division Daughters	Differentiation /Maturation	Active Movement	Signal Production
S (Stem cell)	I. n^+ : $S \rightarrow S + S$ II. n^- Wnt high: $S \rightarrow S + T$ III. n^- Wnt low: $S \rightarrow T + T$	\emptyset	\emptyset	δ : Contact signal
T (Transit amplifying cell)	$T \rightarrow T + T$	I. $T \rightarrow Ap$ II. $T \rightarrow Sp$	\emptyset	\emptyset
Ap (Absorptive progenitor)	I. $Ap \rightarrow Ap + Ap$ II. $Ap \rightarrow Ap + E$ III. $Ap \rightarrow E + E$	\emptyset	\emptyset	\emptyset
Sp (Secretory progenitor)	I. $Sp \rightarrow G + G$ II. $Sp \rightarrow Sp + G$ III. $Sp \rightarrow Sp + Sp$ IV. $Sp \rightarrow Sp + P$	\emptyset	\emptyset	\emptyset
E (Enterocyte)	\emptyset	\emptyset	\emptyset	\emptyset
G (Goblet cell)	\emptyset	\emptyset	\emptyset	\emptyset
P (Paneth cell)	\emptyset	Mature at the crypt base	Downward	Wnt production if mature

Table 1.2: Unique division behaviors, differentiation/maturation processes, active movements, and signal production among cell types. Passive cell movement is present by dividing cells pushing other cells outwards to create space. Active movement is only present among Paneth cells as migration against the WNT gradient. Notch signaling pathway plays a role in stem cell division. The S-S contact signal is not part of the extracellular grid. The n^+ and n^- contact inhibition effect is acquired by observation of neighboring cells.

Chapter 2

Methods

2.1. Evaluation of decision options

The utilization of previous data for future calculations is most effective when a computational model is built around it. The task at hand is to create a complex multipurpose computational model, which replicates the operation of cells in the intestinal crypt. The uniqueness of different cell types in proliferative functions also creates the need for individual modeling, thus creating a set of cell types in the model is necessary. The cell types in question have been detailed previously in section 1.4. For the model to be realistic I programmed both the internal (proliferation/circadian related) functions of the cells and their external communications. Additionally, the code includes functionality to visualize the results. There are many tools available for such modeling, each with a diverse set of strengths, weaknesses and limitations (MATLAB, Simbiology, Julia). The tool of choice was plain C++ programming language (and supplementary libraries) due to its minimal limitations and my personal skillset. In this chapter I describe the working principles of the model, and the algorithms used.

2.2. Grids

The foundation of the model is a two-dimensional grid, representing a one cell layered mammalian intestinal crypt, and the surrounding villi. Every element on the grid represents a cell. There is also an identical sized grid representing the extracellular matter surrounding the corresponding cells. To represent the set of molecules within the cells and the extracellular matrix, I created two struct variables. These structs are stored in the two grids, each implemented as a nested vector (vector<vector<struct>>).

The extracellular struct variables only contain the current signal molecule concentra-

tions. Unlike the extracellular elements, cells are capable of changing positions throughout the simulation, therefore intracellular structs additionally contain an ID variable. (Extracellular movement is modeled as diffusion (figure 2.3), leaving no need for extracellular ID.) I also added a parental ID variable to trace back proliferation origins. The different cell types share the same struct variable, however there is also a differentiating variable embedded for future functions to recognise them individually.

For precision purposes in the model all concentrations were set as “double” variables (64-bit double-precision floating point).

The extracellular matrix -in the model- has two components: Wingless and Int-1 proteins (WNTs) and Bone Morphogenetic Proteins (BMPs). These are described by two opposing gradients that determine the fate of daughter cells or the outcome of differentiation. One end of the gradients is at the origin of the grid (representing the bottom of the crypt), while the other end is at the corners (representing the top of the villus).

WNT concentration is highest at the base of the crypt and approaches zero at roughly halfway to the top of the villus [22]. Experimental measurements in intestinal tissue-like environments report WNT concentrations of 60–100 ng/ml (2–3 nM/ml) in extracellular matter [25]. Assuming uniform distribution of WNTs, the gradient represents concentrations ranging from 8–12 nM/ml to 0 across the matrix. The BMP gradient, on the other hand, is represented only as a ratio on the matrix, and is present throughout the whole crypt-villus complex. In the model, it lacks molecular functionality that would necessitate precise concentration representation.

The grids are prefixed in size. In both human and mouse intestines, the distance between the base of the crypt and the tip of the villus is typically composed of approximately 25 to 50 cellular layers, depending on the exact species and region of the gut [26]. The grid size is set accordingly.

As a step zero, I fill the central area of the grid with cells constituting a starter colony. The composition of the starter colonies may vary both in cell types, and initial concentrations with respect to the different simulations. The pre-filled area is only a fraction of the full grid, providing space for the digital colony to grow. The WNT and BMP gradients also need to be loaded up in the beginning.

The length of the gradients can be calculated from the distance between the origin and the corner cells. The maximum WNT concentration divided by the length of the

gradient gives us the $\Delta WNT/cell$ (WNTpC) value, where *cell* is a unit of length.

$$WNTpC = \frac{WNT_{max}}{\sqrt{2 \cdot \left(\frac{\text{gridsize}}{4}\right)^2}} \quad (2.1)$$

Using this, the unique WNT value is calculated for every cell position, given that the distance is not higher, than the length of the gradient.

$$v[i][j].WNT = WNT_{max} - \text{distance} \cdot WNTpC \quad (2.2)$$

, where

$$\text{distance} = \sqrt{\left(i - \frac{\text{gridsize}}{2}\right)^2 + \left(j - \frac{\text{gridsize}}{2}\right)^2} \quad (2.3)$$

The values *i* and *j* represent the positions in the double vector layout, corresponding to their *row* and *column* indices. They are not equivalent to the position's coordinates in the logical coordinate system. By shifting the coordinate system, the equation simplifies to a Pythagorean theorem.

When the setup of the initial colony is ready, the state altering section of the code begins. This section is a loop, each run symbolising a small time lapse. The number of iterations is pre-set. One iteration goes through several functions to alter the whole colony.

2.3. Working principle

To imitate biological processes in a digital environment I had to break these processes down to a logical order. Modeling and simulating all of a cell's functions is both impossible and unnecessary regarding this project. To avoid excessive computational cost, I selected the molecules and processes important to the research and separated them into computable functions as seen in Figure 2.1.

2.3.1 Cell age counter

Most cells in the villus die naturally. The vast majority of these mortal cells get pushed upwards during proliferation to the top of the villus and shed off. The others die in an apoptotic manner. This process is highly dependent on external factors as well as internal factors making it hard to find its source. Coding the dying process in

Function flow of the cell colony

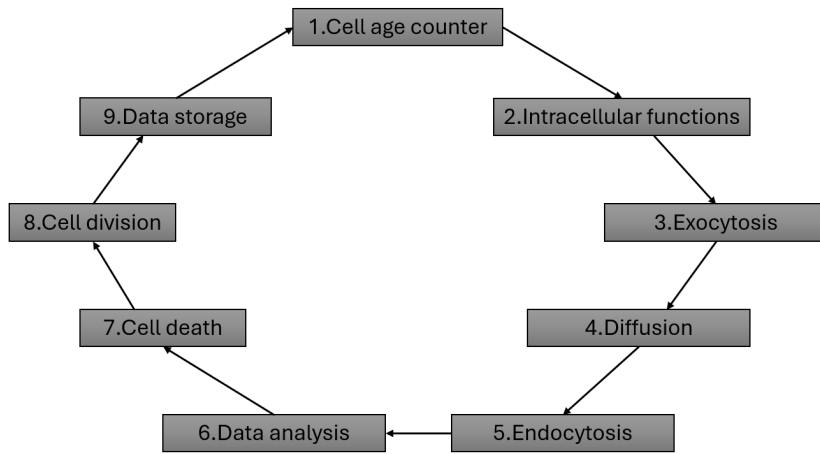


Figure 2.1: Flow chart of the functions. The functions repeat linearly any given number of times. The functions affect the whole grid. A full circle constitutes one step in the model. The number of iterations change based on the simulation's purpose.

Individual cell fate

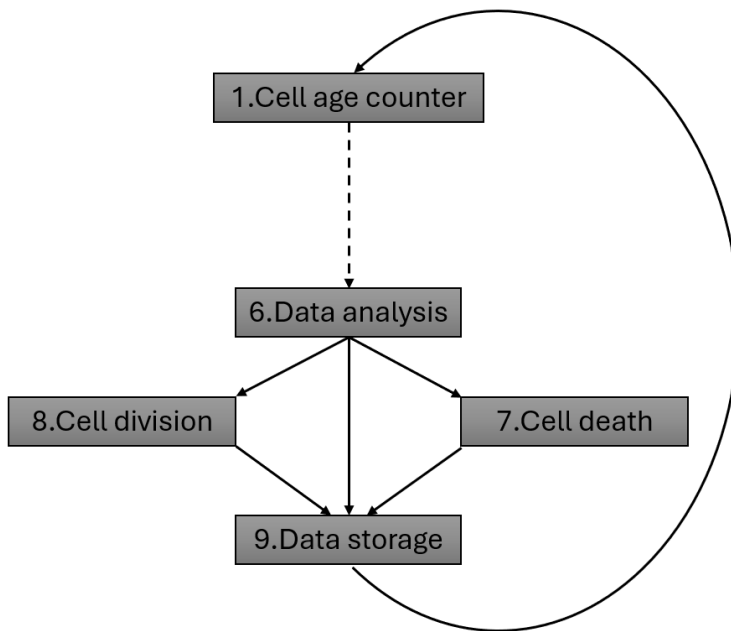


Figure 2.2: Flow chart of individual cell fates. Although the program iterates through all of the functions each run, the individual cells take different paths based on their types and states. The data analysis function decides the fate of each cell and groups them accordingly.

a biologically relevant way would be close to impossible, and unnecessary regarding the project. However, the event itself is important in the representation of proliferation scales and the simulation’s biological relevance. To balance the healthy colony’s self-renewal, I included an age counter for each cell. In some cell types this variable after exceeding a certain threshold highly increases the chance of the cell dying. In other – “immortal”-cell types this number only serves informational purposes.

Each iteration the counters value is increased by 1.

2.3.2 Intracellular functions

Base model

The cells have their own sets of ordinary differential equations (ODEs), derived from internal molecular processes related to cell division or the circadian clock. I utilized a model provided by my supervisor, Dr. Attila Csikász-Nagy, which was published alongside the corresponding article [27]. The cell cycle model is based on the Novák-Tyson model [28] and is coupled with a smaller circadian model.

The regulator of this system is the molecule cyclin B: when its concentration reaches the threshold of 0.002, the cell divides.

First, I translated the model from the .ode format to C++. I defined the constants as global constants and organized the variables within a struct. Since the C++ programming language does not include a built-in ODE solver, I considered importing libraries that offer ODE solver functionalities (e.g., `odeint`). However, the structure of these solutions was not compatible with the rest of the code. Consequently, I implemented a simple ODE solver using explicit Euler’s method. I uploaded the code of the ODE solver to Github available as *Euler ode solver*.

The stochasticity in my model deviates slightly from the original. In the original model, a Wiener process function was used to generate the random variables altering the simulation. Instead of the Wiener process, I implemented random number generation within the range $[-1, 1]$, as seen in equation 2.15. The range is reduced, but the number of possible values is significantly increased compared to the original model.

The system of ODEs used in the model are the following:

$$\frac{d[\text{CYCB}]}{dt} = \varepsilon \cdot \left(K_{1p} + K_1 \cdot \frac{\left(\frac{[\text{CYCB}]}{J_1}\right)^2}{1 + \left(\frac{[\text{CYCB}]}{J_1}\right)^2} \right) \cdot \text{MASS} - V_2 \cdot [\text{CYCB}] (k_{\text{wee1p}} + k_{\text{wee1s}} \cdot [\text{Wee1}]) \\ \cdot [\text{CYCB}] + (k_{\text{cdc25p}} + k_{\text{cdc25s}} \cdot [\text{Cdc25a}]) \cdot [\text{CycBP}] + \text{Noise}_{\text{CYCB}} \quad (2.4)$$

$$\frac{d[\text{CycBP}]}{dt} = (k_{\text{wee1p}} + k_{\text{wee1s}} \cdot \text{Wee1}) \cdot \text{CYCB} - (k_{\text{cdc25p}} + k_{\text{cdc25s}} \cdot \text{Cdc25a}) \cdot \text{CYCET} - V_2 \\ \cdot \text{CYCET} + \text{Noise}_{\text{CYCET}} \quad (2.5)$$

$$\frac{d[\text{Wee1}]}{dt} = (k_{w5p} + k_{w5s} \cdot M) - k_{w6} \cdot \text{Wee1} - \frac{(k_{w2p} + k_{w2s} \cdot \text{CYCB}) \cdot \text{Wee1}}{J_{w2} + \text{Wee1}} + \frac{k_{w1} \cdot \text{Wee1P}}{J_{w1} + \text{Wee1P}} \\ + \text{Noise}_{\text{Wee1}} \quad (2.6)$$

$$\frac{d[\text{Wee1P}]}{dt} = \frac{(k_{w2p} + k_{w2s} \cdot \text{CYCB}) \cdot \text{Wee1}}{J_{w2} + \text{Wee1}} - \frac{k_{w1} \cdot \text{Wee1P}}{J_{w1} + \text{Wee1P}} - k_{\text{wd}} \cdot \text{Wee1P} + \text{Noise}_{\text{Wee1P}} \quad (2.7)$$

$$\frac{d[\text{Cdc25a}]}{dt} = \frac{(k_{c3p} + k_{c3s} \cdot \text{CYCB}) \cdot (1 - \text{Cdc25a})}{J_{c3} + (1 - \text{Cdc25a})} - \frac{k_{c4} \cdot \text{Cdc25a}}{J_{c4} + \text{Cdc25a}} + \text{Noise}_{\text{Cdc25a}} \quad (2.8)$$

$$\frac{d[\text{ERG}]}{dt} = \frac{\varepsilon \cdot k_{15}}{1 + \left(\frac{\text{DRG}}{J_{15}}\right)^2} - k_{16} \cdot \text{ERG} + \text{Noise}_{\text{ERG}} \quad (2.9)$$

$$\frac{d[\text{DRG}]}{dt} = \varepsilon \cdot \left(k_{17p} \cdot \text{ERG} + k_{17} \cdot \frac{\left(\frac{\text{DRG}}{J_{17}}\right)^2}{1 + \left(\frac{\text{DRG}}{J_{17}}\right)^2} \right) - k_{18} \cdot \text{DRG} + \text{Noise}_{\text{DRG}} \quad (2.10)$$

$$\frac{d[\text{CYCD}]}{dt} = \varepsilon \cdot K_9 \cdot \text{DRG} + V_6 \cdot \text{CD} + k_{24r} \cdot \text{CD} - k_{24} \cdot \text{CYCD} \cdot \text{P27} - K_{10} \cdot \text{CYCD} + \text{Noise}_{\text{CYCD}} \\ (2.11)$$

$$\frac{d[\text{CD}]}{dt} = k_{24} \cdot \text{CYCD} \cdot \text{P27} - k_{24r} \cdot \text{CD} - V_6 \cdot \text{CD} - K_{10} \cdot \text{CD} + \text{Noise}_{\text{CD}} \quad (2.12)$$

$$\frac{d[\text{P27}]}{dt} = \varepsilon \cdot K_5 + K_{10} \cdot \text{CD} + k_{24r} \cdot \text{CD} - V_6 \cdot \text{P27} - K_{25} \cdot \text{P27} \cdot (\text{CYCE} + \text{CYCA}) - k_{24} \\ \cdot \text{CYCD} \cdot \text{P27} + K_{25R} \cdot (\text{CE} + \text{CA}) + V_8 \cdot \text{CE} + K_{30} \cdot \text{Cdc20} \cdot \text{CA} + \text{Noise}_{\text{P27}} \\ (2.13)$$

$$\frac{d[\text{Cdc20}]}{dt} = K_{13} \cdot \text{IEP} \cdot \frac{\text{Cdc20i}}{J_{13} + \text{Cdc20i}} - K_{14} \cdot \frac{\text{Cdc20}}{J_{14} + \text{Cdc20}} - K_{12} \cdot \text{Cdc20} + \text{Noise}_{\text{Cdc20}} \quad (2.14)$$

$$\text{Noise}_{[\text{MOLECULE}]} = [\text{RANDOM NUMBER}] \cdot \sqrt{2 \cdot \text{amp} \cdot [\text{MOLECULE}]} \quad (2.15)$$

All supplementary information regarding the ODE system is listed in Appendix A, and the original *.ode* file of the model is also uploaded to my thesis repository on Github as *Circadian coupled cc model*.

Cell division periods vary among the cell types. While transit amplifying cells and absorptive progenitors divide roughly twice as many times as ISCs, secretory progenitors tend to divide half as many times. Division initializer molecules and thresholds are believed to be roughly the same in all cells. To achieve realistic results, instead of manipulating the model, I set it as the division period of the secretory progenitors (48-hour lapse). Every one step the secretory progenitors take, the ISCs take two, and the transit amplifying and absorptive progenitors take four. With this method I sacrifice finding the exact step fast proliferating cells would divide in, providing reduced margin of error in the flow of the model itself. Also, division thresholds in reality are not as strict as they are in a model, making this loss of precision negligible. Note, that only the cell cycle module's steps are manipulated, the circadian module steps only once per iteration in every case.

Conclusively, more rapidly proliferating cell types divide [0; 3] steps after reaching the threshold, with equal distribution. ISCs divide [0;1] steps after reaching the threshold, with equal distribution. Due to the WNT cross effect (equation 2.16) and the noise implemented in the equations, the distribution of the jumps is not biased towards one scenario. Non-proliferative cells don't have the model implemented.

WNT cross effect

Utilizing the WNT gradient, I extended the model to include the effects of WNT signaling on the cell cycle. The extension is minimal, as the primary role of WNT in my simulation model is to define daughter cells and differentiation. Modifying the equations of the cell cycle model could lead to undesired outcomes. Within the intracellular space and equation system, β -catenin is a main intermediary molecule for WNT signaling inside the cell [2]. As β -catenin is not implemented in the original cell cycle model, cyclin B

concentrations (the model's critical regulatory molecule), are coded to be directly affected by the extracellular WNT levels. While the actual effect is significantly more complex, this implementation is sufficient for the current simulation objectives.

In theory there is 360 ng/ml of WNT at the very base of the crypt (calculated in section 2.2):

$$\text{WNT} = 3.6 \cdot 10^{-4} \frac{g}{ml}$$

The average decrease of cyclin B in one step, based on testing is

$$\frac{d\text{CYCB}}{dt} = -1.04167 \cdot 10^{-5}$$

Based on these I could calculate and set the maximum effect of the extracellular WNT gradient on the cell cycle as approximately 10% accelerative. For this effect I use a WNT regulator constant (WR), which I acquired by iterative adjustment. The WNT extended differential equation of cyclin B is

$$\begin{aligned} \frac{d\text{CYCB}}{dt} = & \varepsilon \cdot \left(K1p + K1 \cdot \frac{\text{CYCB}^2}{J1^2 + \text{CYCB}^2} \right) \cdot \text{MASS} - V2 \cdot \text{CYCB} - (kwee1p + kwee1s \cdot \text{Wee1}) \cdot \\ & \text{CYCB} + (kcde25p + kcde25s \cdot \text{Cdc25a}) \cdot \text{CycBP} - \text{WNT} \cdot \text{WR} + \text{Noise}_{\text{CYCB}} \end{aligned} \quad (2.16)$$

, where

$$\text{WR} = 17$$

2.3.3 Exocytosis – Diffusion - Endocytosis

Parallel to molecule interactions taking place in the intracellular matter, some signal molecules are transported in and out of the cells and diffuse in the extracellular matrix. I took apart the membrane transport to three consecutive components: exocytosis, diffusion and endocytosis. Post maturation Paneth cells actively produce WNT ligands, this process is coded by the exocytosis function.

The diffusion function represents the signal flow in the extracellular space. In cell-cell communication a hexagonal layout of cells has more biological relevance than a rectangular one. During the diffusion function a slot in the extracellular grid communicates with six neighbouring slots (figure 2.3). The hexagonal visualization will be representative to

this positioning. The base of the algorithm is a temporary grid. Each slot is calculated individually and is stored in a new identical (but empty) grid, without altering the initial grid. At the end the new temporary grid is set as the main one. The original grid is terminated. The WNT gradient is mainly provided by cells below the surface layer. Respecting this, the base gradient is differentiated from the WNT produced by Paneth cells. Solely Paneth cell produced WNT goes through diffusion, as the base gradient is maintained from external sources. Post diffusion, Paneth cell produced WNT degrades by certain percentage (Paneth cell produced WNT degradation factor), as maintenance. Endocytic processes are yet irrelevant to this model, however its place in the logical order

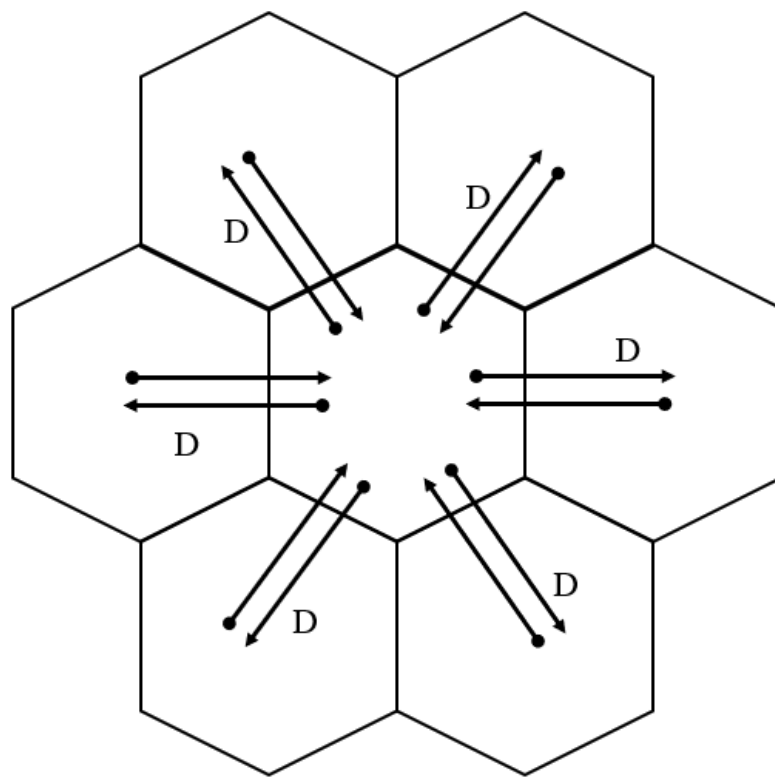


Figure 2.3: Diffusion process illustration. The difference between the middle hexagon and each surrounding one is reduced with the diffusion factor (D) and stored in the temporary grid's corresponding element. Due to the hexagonal layout the indexes of neighbor slots in relation to the middle slot differ based on whether the middle's first grid index is an odd number or not.

is fixed, if ever needed to extend in that direction. (If extracellular WNT wouldn't bypass the intermediate molecule in the code, the communication process would be coded in this function.)

2.3.4 Cell fate analysis

Many factors regulate cell division and cell death (1.2),(1.3). In normal conditions certain molecule concentrations or external factors directly initiate cell division or cell death, but the complex systems cells are, scientific data regarding these initializations is rather theoretical. The utilized model provides data to be processed. This function's task is to determine which cells would divide or die in the current time step. The cells go through an examination process after their internal concentrations and the time has changed. In some cases, if data suggests a certain concentration threshold as initialization, the model implements that. In other cases, without sufficient data available, we calculated a time dependent threshold using the 'cell age counter'. Different cell types show highly different division periods and life spans, the evaluation of cell states reflects that. This section is highly dependent on the data collected and evaluated during project meetings (summarised in Table 1.1) and the cell cycle model detailed in (2.3.2).

Death

The cell types characteristically dying in a natural way are enterocytes, goblet and Paneth cells. When the age of these cells exceeds the lower limit of their average lifespan they begin to gain an increasing probability of dying. From this point, every iteration (representing an hour) they survive increases the chance of them dying in the next. Distinct average lifespan ranges require unique probability calculations. Paneth cells have a rather fluid average lifespan compared to enterocytes and goblet cells, meaning they require a lower probabilities, with a slower build up (1.1).

To acquire concrete numbers I made some calculations. The cell cycle model using a $t=0.005$ time stepper showed an average of 48 iteration/division period during testing. Utilizing this, I considered the unaltered model to be the basis of secretory progenitor cells with a 48h division period meaning, that each iteration represents a one hour time lapse.

The range of lifespan (RoL) in Paneth cells is

$$RoL = 12 \cdot 24 = 288h \quad (2.17)$$

I wanted the probabilities per iteration to sum up to 100% throughout the average lifespan, so I calculated the mean value of the dying probabilities (mDp).

$$mD_{p(p)} = \frac{100}{288} = 0.347\bar{2} \quad (2.18)$$

Provided we start from 0%, the probability-increase with each iteration is

$$\Delta D_{p(p)} = \frac{mD_{p(p)}}{\frac{RoL_p}{2}} = 0,00241\% \quad (2.19)$$

I used the same method for goblet cells and enterocytes as well

$$\Delta D_{p(e,g)} = \frac{mD_{p(e,g)}}{\frac{RoL_{e,g}}{2}} = 0.0868\% \quad (2.20)$$

where

$$RoL_{e,g} = 48h$$

and

$$mD_{p(e,g)} = 2,08\bar{3}$$

This solution leaves very little chance for the cells to surpass the upper bound of their lifespan, but it's still possible (as it is in reality).

Division

I also implemented a stochastic method for cell division, only it is a lot simpler. Once cyclin B decreases below the 0.002 threshold the cell is given a 50% probability of division. This number remains constant throughout further iterations. Due to this simplicity the random number used to determine the cell's division fate in the code is an integer between [0; 9]. Meanwhile determining the cell's death fate required a floating point number, due to high precision demand.

Differentiation

Transit amplifying cells have unique differentiation behaviours. In lower WNT levels they can differentiate into either an absorptive or a secretory progenitor cell. Transit amplifying cells rapidly proliferate, therefore I set a relatively high probability for the event to occur (PoD - probability of differentiation). This value varies, for example from 0% up to 10% depending on the cells position along the WNT gradient. The probability range may depend on simulation objectives.

$$PoD_{p,10} = 10 - \frac{WNT_{local}}{WNT_{max}} \cdot 10 \quad (2.21)$$

Notch signaling pathway is implemented in the determination of the differentiated cell's type.

2.3.5 Death function

The function's input is the container of the cells selected for calculated apoptosis. The selected cells are terminated. During apoptosis the cytoplasm remains contained. The extracellular matter is not altered in the process. After termination the cell's slot remains open.

The process of cells falling off the top of the villi is not coded in a function. As the origin of the grid represents the bottom of an intestinal crypt, the verge of the grid represents the upper parts of one or more villi. Cells simply falling off the grid is a sufficient representation of cells shedding off the villi.

2.3.6 Division function

Division The function's input is the container of coordinates of the cells selected for division or differentiation, and a container of the same cell's ID-s. Using only coordinates makes the function less computationally intensive, however during division processes the layout of the grid changes. To avoid false division matches the function first checks whether the previously contained ID matches the ID of the cell in the corresponding position. If a mismatch is found the function searches the grid for the cell with the right ID and continues working with the new coordinates. This way searching is only required for dislocated cells.

Most cell types have multiple stochastic possibilities of division daughters as seen in Table 1.2. In most cases, the outcome is regulated by signal gradients, other determining factors are unknown. Where sufficient data on determining factors was absent, I used a probabilistic approach based on the ratio of the daughter cells present in a healthy crypt or villus (Table 1.1).

In case of cell differentiation, the cells change types, and reset their age and internal concentrations, without any movement.

The main source of cellular movement is division. The first step of division is checking whether there is a neighboring slot empty. If there is, the division daughter automatically takes up that slot. This is true for both the edges of the colony and the slots left open by cell death. If there is no free space around the cell, other cells get pushed 'up' towards the grid edges. The algorithm deciding the direction of the division is mostly stochastic (Figure 2.4).

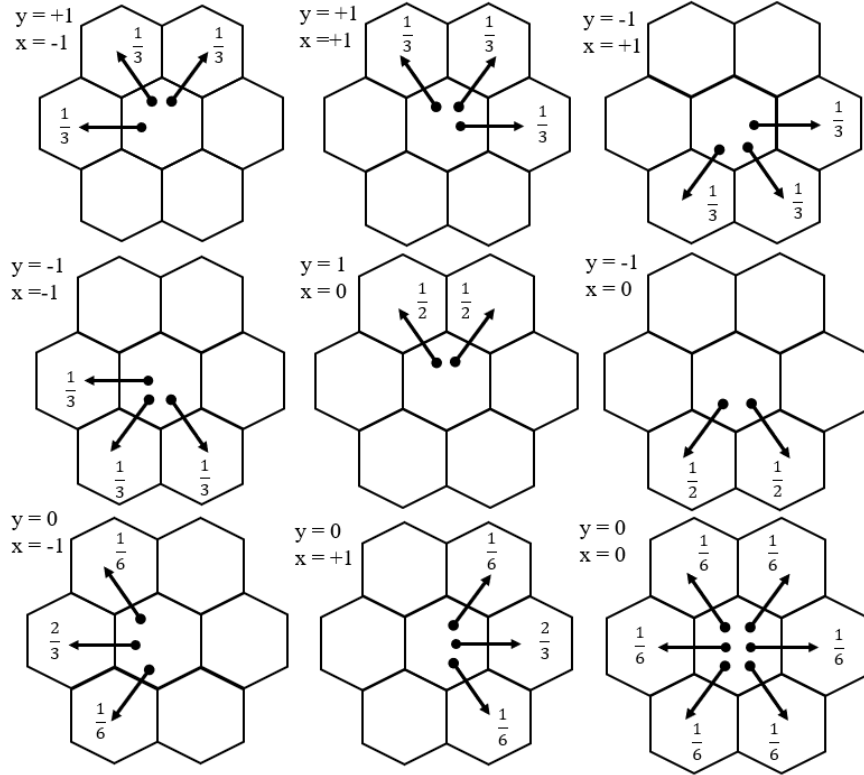


Figure 2.4: The mathematical model of cell movement induced by division. The direction vectors (x, y) relative to the origin at the center of the grid can be determined from a cell's grid indexing. These direction vectors define eight possible movement patterns that ensure the upward flow of cells (toward the edges of the grid). The sum of the probabilities within each category of directions is always 1. The total probability among each of the six directions, combining all eight patterns is equal. If the parent cell is located at the origin $(0, 0)$, it can divide with equal probability in all directions. Indexing movement in odd and even row numbers differs leaving a total of 18 possibility patterns to model.

Migration Discussing migration in the same section as division might seem odd. From a modeling perspective however, its a logical placement as migration is the only other movement inducing function on the grid. Paneth cells are almost always found among, or close to ISCs. They possess the ability to move against the WNT gradient, letting them migrate towards the base of the crypt. This migration is also a maturation process, controlled by the WNT gradient in the crypt. To replicate the migration, a chance-based switching algorithm was implemented in the model, unique to Paneth cells. Paneth cells have a 5% probability to switch positions with their neighbouring cell closest to the origin. Whether this process comes before or after the division is irrelevant.

2.4. Visualization

Following alterations in containers with such large number of elements requires visualization. To sustain information about the grids we can save the current states in each iteration. Depending on simulation objective we can create images representing the grid in certain states, based on a variety of parameters. I used MFC, the built in visualization library of Visual Studio.

Chapter 3

Results

Each simulation has its unique set of parameters implemented in the model. The latest script used for simulating, as well as the ODE solver code and the original model source is available in my *thesis_simulation_codes* repository on Github. The visualization of the data is dependent on the MFC extension of Visual Studio, which is not included in the default installation package. Outside of visualization the script should be compatible with any major compiler.

Please note, that at this stage odd numbered grid sizes might result in unintended simulation outcomes due to limitations of integer types properties. Also note, that *Simulation 1* and *Simulation 2* use pseudo random number generation, meaning the result of running the simulation is deterministic in nature for each parameter set. This means running the script of Simulation 1 and 2 in any computer any time would produce the same exact results as seen in (3.2)(3.3). The first real stochastic simulation is *Simulation 3*.

3.1. Simulation 1

Optimizing the models parameters requires testing. Some of the pre-set parameters have been mentioned earlier in chapter 2, but not all. Parameters such as probabilities of dying are fixed, as changing them would contradict with the relevant literature. Consider them as default settings of the simulation (2.3.4). Extracellular gradient values will also remain unchanged as well as parameters regarding the cell cycle model (2.2)(2.3.2).

The size of the grid is also somewhat calculated from the distance between the peak of the villus and the bottom of the crypt, however the number of cells in these areas are fluid enough to leave room for adjustment if needed.

Parameter Description	Symbol	Value
Grid size	gridsize	60
WNT regulator constant	WR_{10}	17
WNT_p degradation factor	pWNTDF	0.2 (20% degradation/iteration)
Diffusion rate of WNT_p	$D_{f,p}$	0.4
Secretory progenitor division daughter determinator	SPDDD	55%
Rate of Paneth cell WNT secretion post maturation (as a fraction of WNT_{max})	$R_{WNT,p}$	9×10^{-5} (5%)
Minimal distance from origin for Paneth cells to mature	d_{mature}	25 cells
Probability of migration of a Paneth cell per iteration	P_m	0-10%
Probability range of transit amplifying cell differentiation	P_{TA}	0-10%
Minimal number of neighboring ISCs or TAs for n^+ signal (TA cells)	n_{ap}^+	4
Minimal number of neighboring ISCs for n^+ signal (ISCs)	n_s^+	6
WNT threshold for stem cell differentiation	$WNT_{threshold}$	$WNT_{max} - 3 \cdot WNTpC$
Initial number of ISCs in starter colony	N_{ISC}	13
Chance of E + E division (absorptive progenitors)	P_{E+E}	50%
Number of iterations	N_{it}	1000

Table 3.1: Adjustable parameters of Test simulation

The WNT gradient is precisely calculated, but the constant supporting the 10% impact of WNT in intracellular functions in the origin of the grid is only a hypothesis, making it highly adjustable.

The constant SPDDD (secretory progenitor division daughter determinator) repre-

sents the chance each division pattern has to be chosen as opposed to all the other patterns further down the line. Adjusting this requires caution not to go below 50%. If we did, the probability of the second last pattern would become smaller than the probability of the last due to the system's nature.

If there is no contact inhibition nor differentiation signal, stem cells automatically follow the S + T division pattern.

Absorptive progenitors have a fixed 50% chance to follow the E + E division pattern. The probabilities of the other two patterns complement each other, leaning towards one based on BMP levels, introducing inequality at the colony level due to the grid shape (Table 3.1).

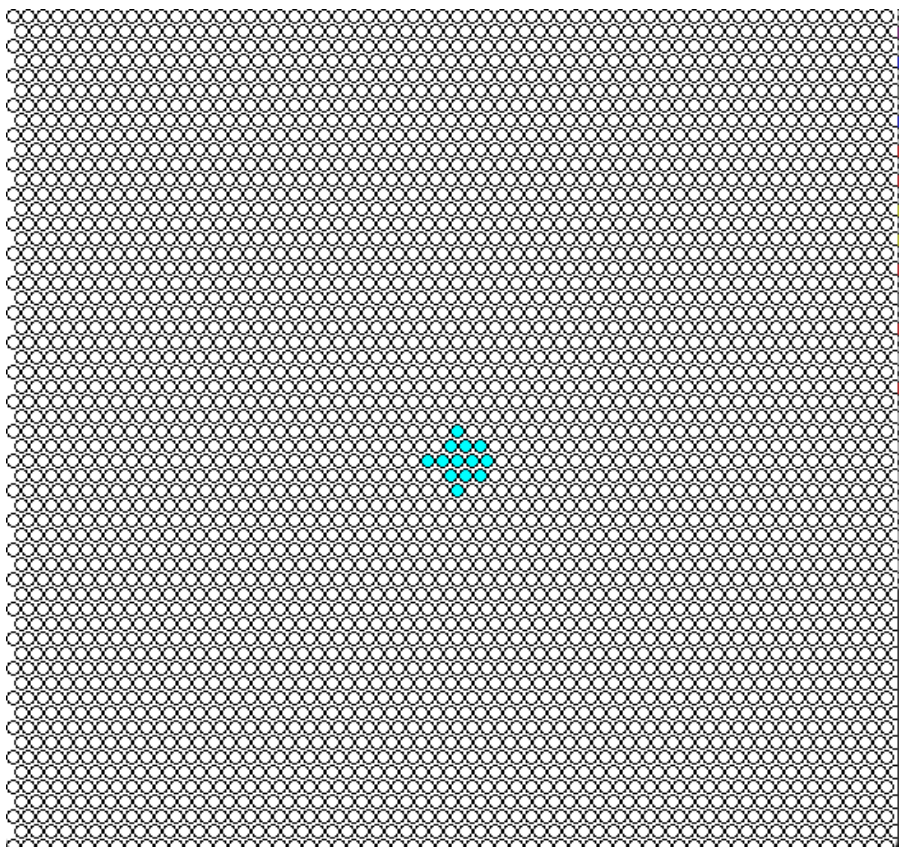


Figure 3.1: Initial stem cell colony. Inconsistent form is due to the usage of distance-from-origin based uploading. Distance calculations are derived from grid indexing, not taking the hexagonal layout into account. Grid indexing starts from the top left corner with $(0,0)$.

3.1.1 Evaluation of Simulation 1

At this stage visual cues provide sufficient feedback on the model.

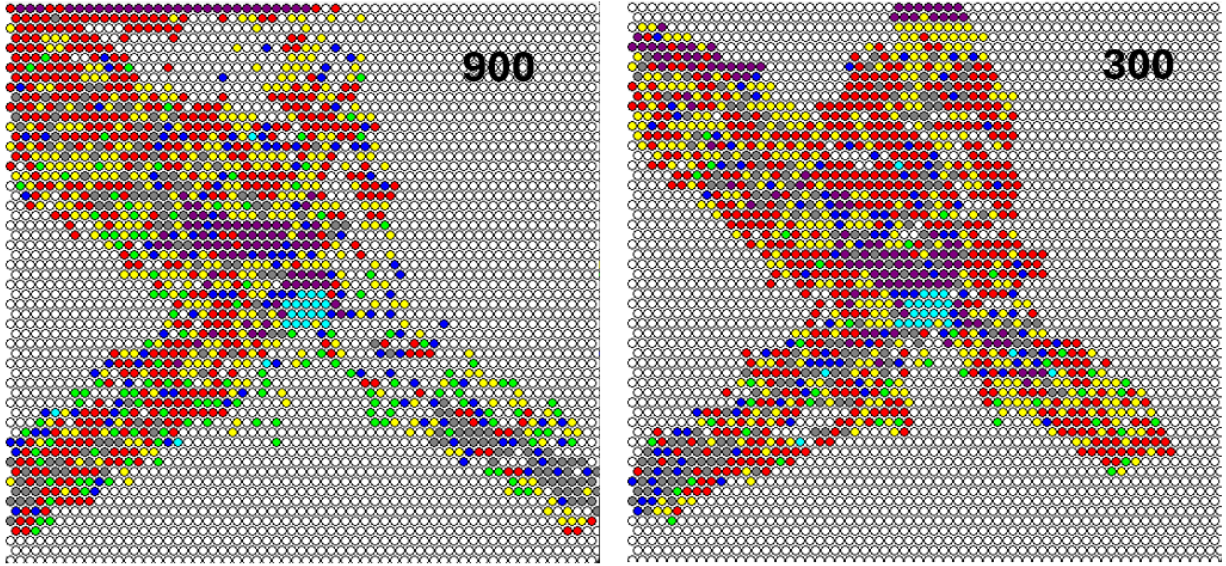


Figure 3.2: Simulation 1 grid states after 300 and 900 iterations. Color scheme: ISCs-cyan, TAs-purple, absorptive progenitors-blue, secretory progenitors-yellow, goblet cells-red, enterocytes-grey, Paneth cells-green, empty positions-white.

The size of the colony grows quickly in the beginning, however slows down after 300 iterations (Figure 3.2). The number of enterocytes is visibly low. The increasing number of open slots near the stem cell niche suggests an inconsistency between death and division timers. High numbers of TA cells near the edges of the grid are unnatural as they mostly should have differentiated already or fell off. The number of Paneth cells is also higher than expected. Asymmetrical division arrangement suggest biased movement.

3.2. Simulation 2

To increase division near the stem cell niche I doubled the WNT regulator constant for higher impact (Table 3.2). I increased the overall probability of $E + E$ division pattern among absorptive progenitors and implemented distance-from-origin dependency as well (meaning I suggest an extracellular gradient might manipulate the division daughters). I altered the boundary conditions regarding TA cell differentiation, and increased the secretory progenitor division daughter determinator value based on the number of Paneth cells. A logical error in the script was corrected promoting a more symmetrical alignment.

3.2.1 Evaluation of Simulation 2

Lateral division patters still seem to dominate over vertical ones (Figure 3.3). (The visualization is rotated with a 90° angle to the right in comparison to the code. Lateral

Symbol	Value
WR_{10}	34
P_{E+E}	50%-80%
SPD3D	60%

Table 3.2: Parameters of Simulation 2 adjusted based upon evaluation of Simulation 1. Parameters not listed remained unchanged (3.1).

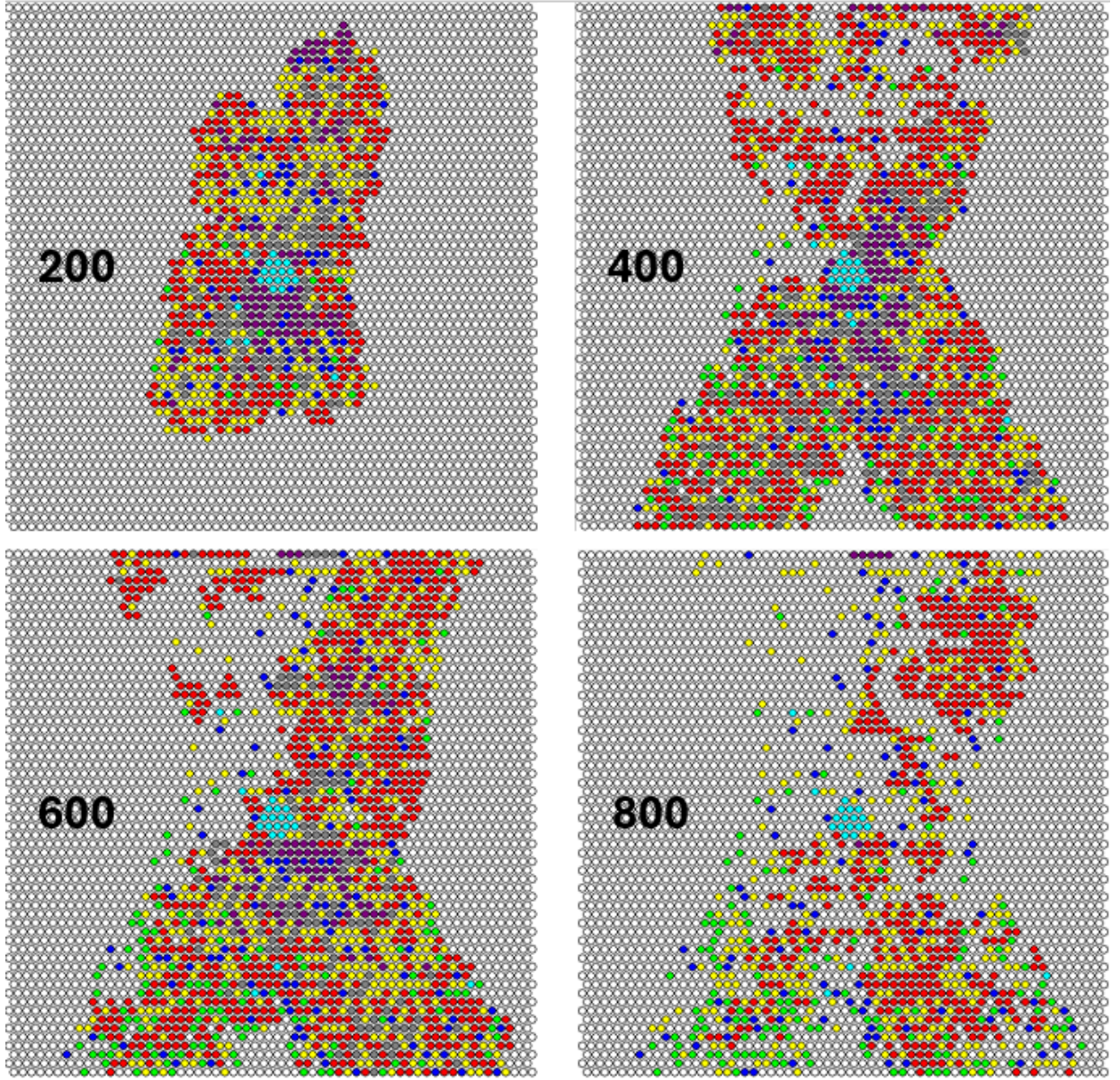


Figure 3.3: Simulation 2 grid states after 200, 400, 600 and 800 iterations. Color scheme: ISCs-cyan, TAs-purple, absorptive progenitors-blue, secretory progenitors-yellow, goblet cells-red, enterocytes-grey, Paneth cells-green, empty positions-white.

division patterns produce vertical alterations in the figures.) Characteristic X shape persists. Low number of TA cells coupled with the deterioration of colony density suggests TA cells differentiate in higher volumes than they are being produced resulting in a deficit of proliferating cells. Lower TA density also leads to low number of them self-replicating.

3.3. Simulation 3

After revision of the functions coding movement patterns I concluded that the characteristic X shape is a byproduct of the C++ integrated random number generator functions bias. In this simulation I transformed every probabilistic process to stochastic, by only using the *random* library offered generators, and embedding the actual time as its seed.

I also lowered the probability of transit amplifying cell differentiation to 2.5% per iteration on average (Table 3.3).

Symbol	Value
P_{TA}	0-5%
Randomized processes	Deterministic \rightarrow Stochastic

Table 3.3: Parameters of Simulation 3 adjusted based upon evaluation of Simulation 1 and 2. The value of parameters not listed are equivalent to the values of parameters of Simulation 2 (3.2).

3.3.1 Evaluation of Simulation 3

Number and positions of TA cells are promising (Figure 3.4). Proliferation is still insufficient to upload the entire grid. Most Paneth cells are positioned in areas near the edges suggesting that migration movements towards the niche are slow compared to the push-out effect of division. Number of secretory progenitors is also high compared to absorptive progenitors.

3.4. Simulation 4

For this simulation I accelerated Paneth cell migration. Other division acceleratory changes have not been set, due to the WNT production of matured Paneth cells. For

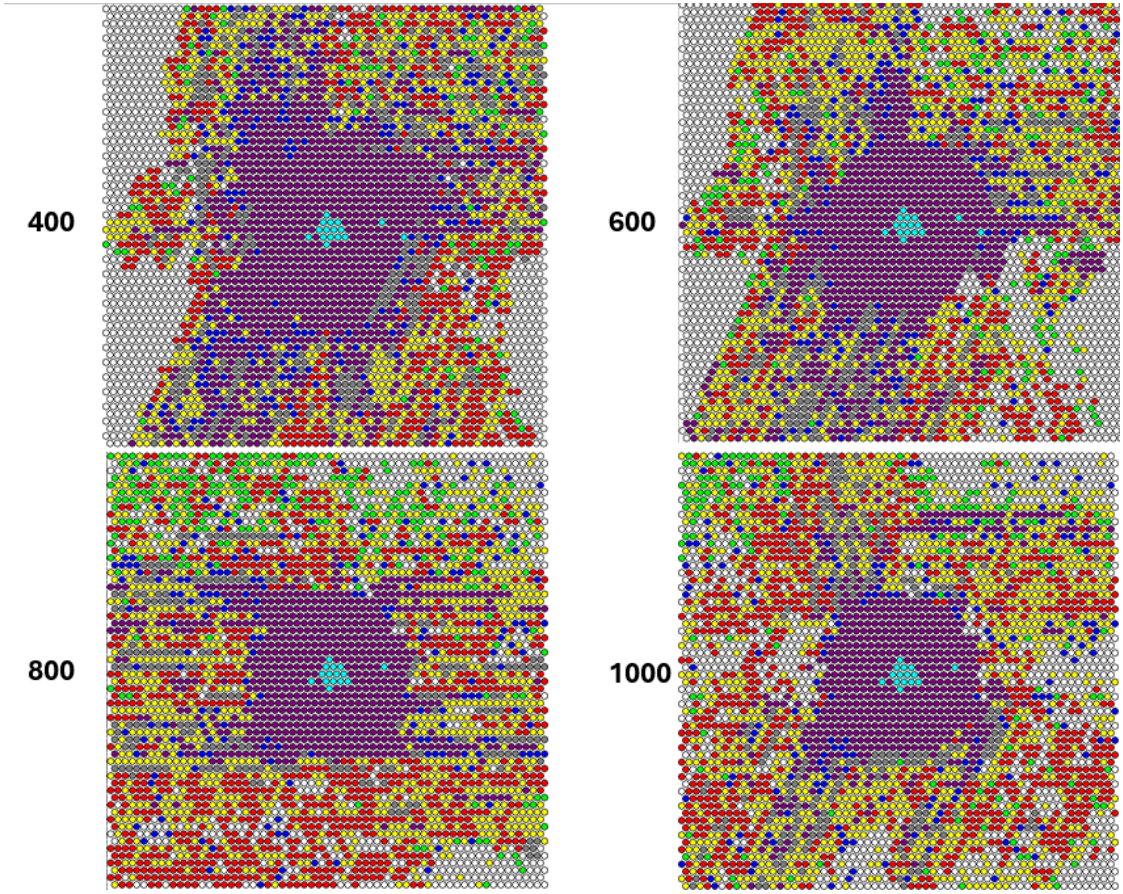


Figure 3.4: Simulation 3 grid states after 400, 600, 800 and 1000 iterations. Color scheme: ISC_s-cyan, TAs-purple, absorptive progenitors-blue, secretory progenitors-yellow, goblet cells-red, enterocytes-grey, Paneth cells-green, empty positions-white.

handling progenitor imbalance I lowered the threshold of n^+ signal in TA cell differentiation(Table 3.4).

Symbol	Value
n_{ap}^+	2
P_m	0-15%

Table 3.4: Parameters adjusted for Simulation 4. Parameters not listed are unchanged.

3.4.1 Evaluation of Simulation 4

The total number of cells that turn up on the grid, including dead ones is 37.000. Paneth cells stuck near the edges causing proliferation to fall back again. The average population loss off cells between 500 and 1000 iterations is around 9% (Table 3.5). The ratio between absorptive progenitors and secretory progenitors is sufficient. Their

Cell type	$S_{4.1}$ 500 iterations	$S_{4.1}$ 1000 iterations	$S_{4.2}$ 500 iterations	$S_{4.2}$ 1000 iterations
Number of ISCs	13	13	11	11
Number of TAs	1029	946	1151	880
Number of APs	533	546	405	435
Number of SPs	490	474	287	326
Number of Ps	32	109	39	23
Number of Gs	591	643	647	556
Number of Es	536	208	323	388
Sum	3224	2939	2863	2619
Relative ratio	100%	91.16%	100%	91.48%

Table 3.5: Comparison of two runs. Data derived from Simulation 4 at 500 and 1000 iterations.

numbers are also close to sufficient. The number of transit amplifiers, is too high. The number of enterocytes shows high deviation in relation to time in $S_{4.1}$, and stays consistently below the sufficient range in $S_{4.2}$. This problem might root from the grid not being satiated, meaning a lack of maintenance regarding enterocyte levels caused by the imbalance between death and differentiation processes (Figure 3.5). The number of goblet cells is too high. The number of Paneth cells also shows high deviation from simulation to simulation.

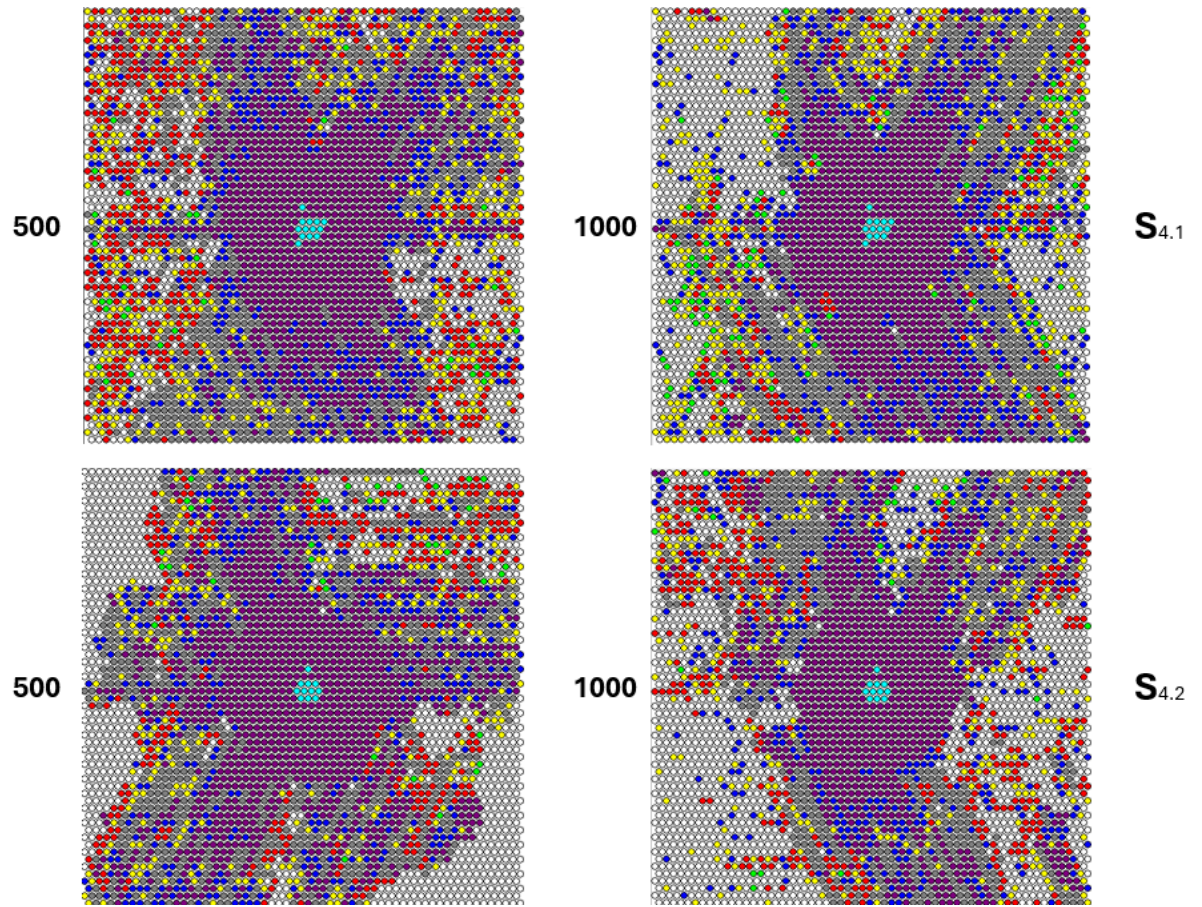


Figure 3.5: Comparison of two simulations with equal parameters of Simulation 4. Color scheme: ISCs-cyan, TAs-purple, absorptive progenitors-blue, secretory progenitors-yellow, goblet cells-red, enterocytes-grey, Paneth cells-green, empty positions-white.

Chapter 4

Summary

4.1. Results

The model is still under development and it shows. Calibrating a model like such is not an easy task due to the high number of undiscovered relations and calibration dependent variables.

Even though high iteration simulation tends to show faulty results compared to an *in vivo* epithelial tissue, overall the modeling framework is functioning, expandable and can be fine tuned.

Circadian signaling pathways have been successfully implemented in the model, along with the related extracellular signal transduction. Altering the parameters related to WNT effects in simulations demonstrated one of the ways a faulty circadian system can disrupt the regulation of cell proliferation. Comparing the results to real life data showed the model does not represent a healthy living tissue yet. Based on this comparison, the model is not yet capable of producing data sufficiently relevant to draw conclusions about the interplay between the cell cycle and circadian rhythms.

4.2. Future plans

4.2.1 Room for improvement

The base circadian rhythm coupled cell cycle model can be improved with time as more information surfaces on the internal processes and the cross effects. The circadian module can be expanded for a more diverse behavior analysis.

The values I calculated regarding the functions and WNT integration might need

deeper more precise calculations. Also extracellular gradient calculations didn't follow the hexagonal layout, meaning WNT and BMP values have smaller inconsistencies in a two dimensional plain.

BMP gradient could be more realistic, the model could include the diffusive BMP signal producton of enterocytes. Other signaling pathways and gradients may be included in the model (e.g. Hedgehog gradient).

The codes could be more documented and implemented in a more object oriented way.

4.2.2 Project future

If the professors overseeing this project find my contributions valuable, I would be eager to continue working on it. I sincerely hope that this project will ultimately advance human knowledge and contribute to improving the world. Even if it achieves this in a small way, I will have no regrets about dedicating my time and efforts to it.

Bibliography

- [1] B. Zhao *et al.*, “Circadian rhythms and colorectal cancer: From cell biology to therapy,” *Cellular and Molecular Life Sciences*, vol. 78, no. 9, pp. 4097–4113, 2021. DOI: [10.1007/s00018-021-03793-y](https://doi.org/10.1007/s00018-021-03793-y).
- [2] T. Matsu-Ura *et al.*, “Interplay between circadian clocks and the cell cycle in adult stem cell differentiation,” *Nature Communications*, vol. 7, p. 11807, 2016. DOI: [10.1038/ncomms11807](https://doi.org/10.1038/ncomms11807).
- [3] J. Massagué, “G1 cell-cycle control and cancer,” *Nature*, vol. 432, no. 7015, pp. 298–306, 2004. DOI: [10.1038/nature03094](https://doi.org/10.1038/nature03094).
- [4] C. J. Sherr, “Cancer cell cycles,” *Science*, vol. 274, no. 5293, pp. 1672–1677, 1996. DOI: [10.1126/science.274.5293.1672](https://doi.org/10.1126/science.274.5293.1672).
- [5] P.-P. S. Cardinali DP Brown GM, “Chronotherapy,” *Pubmed*, 2021. DOI: [10.1016/B978-0-12-819975-6.00023-6](https://doi.org/10.1016/B978-0-12-819975-6.00023-6).
- [6] R. Boutros *et al.*, “Cell cycle regulation by the apc/c in development and disease,” *Nature Reviews Molecular Cell Biology*, vol. 7, no. 11, pp. 756–766, 2006. DOI: [10.1038/nrm1988](https://doi.org/10.1038/nrm1988).
- [7] M. Malumbres and M. Barbacid, “Cyclin-dependent kinases: A family portrait,” *Nature Cell Biology*, vol. 11, no. 11, pp. 1275–1276, 2009. DOI: [10.1038/ncb1109-1275](https://doi.org/10.1038/ncb1109-1275).
- [8] E. Israels and L. Israels, “The cell cycle,” *The Oncologist*, vol. 5, no. 6, pp. 510–513, Dec. 2000, ISSN: 1083-7159. DOI: [10.1634/theoncologist.5-6-510](https://doi.org/10.1634/theoncologist.5-6-510). eprint: https://academic.oup.com/oncolo/article-pdf/5/6/510/41837356/oncolo_5_6_510.pdf. [Online]. Available: <https://doi.org/10.1634/theoncologist.5-6-510>.

- [9] J. Bass and J. S. Takahashi, “Circadian integration of metabolism and energetics,” *Science*, vol. 330, no. 6009, pp. 1349–1354, 2010. DOI: [10.1126/science.1195027](https://doi.org/10.1126/science.1195027).
- [10] C. L. Partch, C. B. Green, and J. S. Takahashi, “Molecular architecture of the mammalian circadian clock,” *Trends in Cell Biology*, vol. 24, no. 2, pp. 90–99, 2014. DOI: [10.1016/j.tcb.2013.07.002](https://doi.org/10.1016/j.tcb.2013.07.002).
- [11] H. Clevers, “The intestinal crypt, a prototype stem cell compartment,” *Cell*, vol. 154, no. 2, pp. 274–284, 2013. DOI: [10.1016/j.cell.2013.07.004](https://doi.org/10.1016/j.cell.2013.07.004).
- [12] S. Malijauskaitė, S. Connolly, D. Newport, and K. McGourty, “Gradients in the in vivo intestinal stem cell compartment and their in vitro recapitulation in mimetic platforms,” *Cytokine Growth Factor Reviews*, vol. 60, pp. 76–88, 2021, ISSN: 1359-6101. DOI: <https://doi.org/10.1016/j.cytogfr.2021.03.002>. [Online]. Available: <https://www.sciencedirect.com/science/article/pii/S1359610121000277>.
- [13] P. Janich *et al.*, “The circadian molecular clock creates epidermal stem cell heterogeneity,” *Nature*, vol. 480, no. 7376, pp. 209–214, 2011. DOI: [10.1038/nature10649](https://doi.org/10.1038/nature10649).
- [14] C. Wallaeys, N. Garcia-Gonzalez, and C. Libert, “Paneth cells as the cornerstones of intestinal and organismal health: A primer,” *EMBO Molecular Medicine*, vol. 15, no. 2, e16427, Feb. 2023, Epub ahead of print: 2022-12-27. DOI: [10.15252/emmm.202216427](https://doi.org/10.15252/emmm.202216427). eprint: 2022-12-27.
- [15] H. Clevers and L. V. D. Flier, “Stem cells, self-renewal, and differentiation in the intestinal epithelium,” *Annual Review of Physiology*, vol. 71, pp. 241–260, 2009. DOI: [10.1146/annurev.physiol.010908.163145](https://doi.org/10.1146/annurev.physiol.010908.163145).
- [16] J. Beumer and H. Clevers, “Cell fate specification and differentiation in the adult mammalian intestine,” *Nature Reviews Molecular Cell Biology*, vol. 22, pp. 39–53, 2021. DOI: [10.1038/s41580-020-0278-0](https://doi.org/10.1038/s41580-020-0278-0).
- [17] L. L. BS Sailaja XC He, “The regulatory niche of intestinal stem cells,” *Journal of Physiology*, vol. 594, pp. 4827–4843, 2016. DOI: [10.1113/JP271931](https://doi.org/10.1113/JP271931).
- [18] T. Yen and N. Wright, “The gastrointestinal tract stem cell niche,” *Stem Cell Reviews*, vol. 2, pp. 203–210, 2006. DOI: [10.1007/s12015-006-0048-1](https://doi.org/10.1007/s12015-006-0048-1).

- [19] K. Kishida, S. Pearce, S. Yu, and N. Gao, “Nutrient sensing by absorptive and secretory progenies of small intestinal stem cells,” *American Journal of Physiology-Gastrointestinal and Liver Physiology*, vol. 312, G111–G117, 2017. DOI: [10.1152/ajpgi.00416.2016](https://doi.org/10.1152/ajpgi.00416.2016).
- [20] K. Z. e. a. A Wu B Yu, “Transmissible gastroenteritis virus targets paneth cells to inhibit the self-renewal and differentiation of lgr5 intestinal stem cells via notch signaling,” *Cell Death Differentiation*, vol. 27, pp. 2520–2532, 2020. DOI: [10.1038/s41419-020-2233-6](https://doi.org/10.1038/s41419-020-2233-6).
- [21] N. Gassler, “Paneth cells in intestinal physiology and pathophysiology,” *World Journal of Gastrointestinal Pathophysiology*, vol. 8, pp. 150–160, 2017. DOI: [10.4291/wjgp.v8.i4.150](https://doi.org/10.4291/wjgp.v8.i4.150).
- [22] A. Baillies, N. Angelis, and V. S. W. Li, “Hallmarks of intestinal stem cells,” *Development*, vol. 147, no. 15, dev182675, Aug. 2020, ISSN: 0950-1991. DOI: [10.1242/dev.182675](https://doi.org/10.1242/dev.182675). eprint: <https://journals.biologists.com/dev/article-pdf/147/15/dev182675/3481875/dev182675.pdf>. [Online]. Available: <https://doi.org/10.1242/dev.182675>.
- [23] P. Buske, J. Galle, N. Barker, G. Aust, H. Clevers, and M. Loeffler, “A comprehensive model of the spatio-temporal stem cell and tissue organisation in the intestinal crypt,” *PLOS Computational Biology*, vol. 7, no. 1, pp. 1–13, Jan. 2011. DOI: [10.1371/journal.pcbi.1001045](https://doi.org/10.1371/journal.pcbi.1001045). [Online]. Available: <https://doi.org/10.1371/journal.pcbi.1001045>.
- [24] L. Gall, C. Duckworth, F. Jardi, *et al.*, “Homeostasis, injury, and recovery dynamics at multiple scales in a self-organizing mouse intestinal crypt,” *eLife*, vol. 12, M. Gómez-Schiavon, A. M. Walczak, and M. Gómez-Schiavon, Eds., e85478, Dec. 2023, ISSN: 2050-084X. DOI: [10.7554/eLife.85478](https://doi.org/10.7554/eLife.85478). [Online]. Available: <https://doi.org/10.7554/eLife.85478>.
- [25] A. A. Ahmad, Y. Wang, C. E. Sims, S. T. Magness, and N. L. Allbritton, “Optimizing wnt-3a and r-spondin1 concentrations for stem cell renewal and differentiation in intestinal organoids using a gradient-forming microdevice,” *RSC Adv.*, vol. 5, pp. 74881–74891, 91 2015. DOI: [10.1039/C5RA14923A](https://doi.org/10.1039/C5RA14923A). [Online]. Available: <http://dx.doi.org/10.1039/C5RA14923A>.
- [26] V. Bonis, C. Rossell, and H. Gehart, “The intestinal epithelium – fluid fate and rigid structure from crypt bottom to villus tip,” *Frontiers in Cell and Developmental Bi-*

- ology*, vol. 9, 2021, ISSN: 2296-634X. DOI: [10.3389/fcell.2021.661931](https://doi.org/10.3389/fcell.2021.661931). [Online]. Available: <https://www.frontiersin.org/journals/cell-and-developmental-biology/articles/10.3389/fcell.2021.661931>.
- [27] J. Zámborszky, C. I. Hong, and A. Csikász-Nagy, “Computational analysis of mammalian cell division gated by a circadian clock: Quantized cell cycles and cell size control,” *Journal of Biological Rhythms*, vol. 22, no. 6, pp. 542–553, 2007. DOI: [10.1177/0748730407307225](https://doi.org/10.1177/0748730407307225).
 - [28] B. Novák and J. J. Tyson, “A model for restriction point control of the mammalian cell cycle,” *Journal of Theoretical Biology*, vol. 230, no. 4, pp. 563–579, Oct. 2004. DOI: [10.1016/j.jtbi.2004.04.039](https://doi.org/10.1016/j.jtbi.2004.04.039).
 - [29] F. Máté, *Base model*, https://github.com/fulmat/thesis/blob/3edc62dfd78b792cfeba50a280adc774e8a2779f/Circadian_coupled_cell_cycle_model.ode.

Appendix A

Supplementary data of the implemented cell cycle model [29]

Equation	Description
$V_4 = K_4 \cdot (G_E \cdot CYCE + G_A \cdot CYCA + G_B \cdot CYCB)$	Cdh1 inactivation rate
$V_6 = K'_6 + K_6 \cdot (H_E \cdot CYCE + H_A \cdot CYCA + H_B \cdot CYCB)$	p27 degradation rate
$V_8 = K'_8 + K_8 \cdot \frac{Y_E(CYCE+CYCA)+Y_BCYCB}{J_8+CYCET}$	CycE degradation rate
$PP1A = \frac{PP1T}{K_{21} \cdot (F_E(CYCE+CYCA)+F_B \cdot CYCB) + 1}$	Active PP1 calculation
$RBH = \frac{RBT}{K_{20} \cdot \frac{L_DCYCDT + L_ECYCE + L_ACYCA + L_BCYCB}{K'_{19}(PP1T - PP1A) + K_{19}PP1A} + 1}$	Hypo-phosphorylated Rb
$E2FA = \frac{(E2FT - E2RBC) \cdot E2F}{E2FT}$	Active E2F calculation
$V_2 = K'_2 \cdot (1 - Cdh1) + K_2 Cdh1 + K''_2 Cdc20$	CycB degradation rate
$L = \frac{K_{26R} + K_{20}(LD \cdot CYCDT + LE \cdot CYCE + LA \cdot CYCA + LB \cdot CYCB)}{K_{26}}$	Rb complex factor
$E2RBC = \frac{2 \cdot E2FT \cdot RBH}{E2FT + RBH + L + \sqrt{(E2FT + RBH + L)^2 - 4 \cdot E2FT \cdot RBH}}$	E2F-Rb complex calculation

Table A.1: Intermediate equations / calculated values of the ODEs

Variable	Initial Value	Variable	Initial Value	Variable	Initial Value
Wee1	2.3	Wee1P	0.077	Cdc25a	0.016
CycB	0.0025	CycBP	0.0028	ERG	0.01218
DRG	0.90053	CYCD	0.01288	CD	0.4343
CYCE	0.01693	CE	0.4828	CYCA	0.00146
CA	0.04038	P27	0.84912	Cdh1	0.99
PPX	1	IEP	0.000017	Cdc20	0.00001
Cdc20i	0.00009	E2F	4.957	GM	0.938
MASS	1.076	eps	1	oszt	8
M	1.4	CP	0.037	CP2	0.046
TF	0.13				

Table A.2: Initial values of the system variables

Parameter	Value	Parameter	Value	Parameter	Value	Parameter	Value
kw5'	0.25	kw5''	2	kw6	1	kw2'	0.2
kw2''	2	Jw2	0.2	kw1	0.4	Jw1	0.2
kwd	1	kc3'	0.1	kc3''	1	Jc3	0.05
Jc4	0.05	kc4	0.4	K1'	0.1	K1	0.6
J1	0.1	K2'	0.05	K2	20	K2''	1
kweel'	0.08	kweel''	10	kcdc25'	0.05	kcdc25''	10
k15	0.25	k16	0.25	J15	0.1	k17'	0.35
k17	10	J17	0.3	k18	10	K9	2.5
K10	5	k24	1000	k24r	10	K7'	0
K7	0.6	K8'	0.1	K8	2	K25	1000
K25R	10	J8	0.1	YE	1	YB	0.05
K29	0.05	K30	20	K5	20	K6'	10
K6	100	HE	0.5	HB	1	HA	0.5
RBT	10	LD	3.3	LE	5	LB	5
LA	3	K20	10	K19'	0	K19	20
K21	1	PP1T	1	FE	25	FB	2
K3'	7.5	K3	140	J3	0.01	J4	0.01
K4	40	GE	0	GB	1	GA	0.3
K33	0.05	K34	0.05	K31	0.7	K32	1.8
J31	0.01	J32	0.01	K13	5	K14	2.5
J13	0.005	J14	0.005	K11'	0	K11	1.5
K12	1.5	E2FT	5	K22	1	K23'	0.005
K23	1	K26	10000	K26R	200	K27	0.2
K28	0.2	MU	0.033	Kez	0.2	DEPRIV	-10
n	2	J	0.3	kms	1	kmd	0.1
kcps	0.5	kcpd	0.525	ka	100	kd	0.01
kp1	10	kcp2d	0.0525	kicd	0.01	kica	20
kp2	0.1	Jp	0.05	TFtot	0.5		

Table A.3: Constant parameter values used in the equations